Multimodal Theranostic Cyanine-Conjugated Gadolinium(III) Complex for In Vivo Imaging of Amyloid-β in an Alzheimer's Disease Mouse Model

Wang, Xueli; Chan, Hei Nga; Desbois, Nicolas; Gros, Claude P.; Bolze, Frédéric; Li, Yinhui; Li, Hung Wing; Wong, Man Shing

Published in:
ACS Applied Materials and Interfaces

DOI:
10.1021/acsami.1c01585

Published: 28/04/2021

Document Version:
Peer reviewed version

Multimodal Theranostic Cyanine-Conjugated Gadolinium (III) Complex for *In Vivo* Imaging of Amyloid-β in Alzheimer's Disease Mouse Model

Xueli Wang,[1] Hei Nga Chan,[1] Nicolas Desbois,[2] Claude P. Gros,[2] Frédéric Bolze,[3]* Yinhui Li,[4]* Hung Wing Li,[5]* Man Shing Wong[1]**

1. Department of Chemistry, Hong Kong Baptist University, Kowloon Tong, Hong Kong, SAR China. E-mail: mswong@hkbu.edu.hk

2. ICMUB (UMR CNRS 6302), Université Bourgogne Franche-Comté, 21000 Dijon, France. E-mail: Claude.Gros@u-bourgogne.fr

3. Conception et Applications des Molécules Bioactives (UMR CNRS-Unistra 7199), Faculté de Pharmacie, Université de Strasbourg, 74 route du Rhin, 67401 Illkrich, France. E-mail: frederic.bolze@unistra.fr

4. Key Laboratory for Green Organic Synthesis and Application of Hunan Province, Key Laboratory of Environmentally Friendly Chemistry Application of Ministry of Education, College of Chemistry, Xiangtan University, Xiangtan 411105, China. Email: yinhuili16@163.com

5. Department of Chemistry, The Chinese University of Hong Kong, Shatin, Hong Kong, SAR China. E-mail: hungwingli@cuhk.edu.hk

KEYWORDS. Gadolinium (III) complex-cyanine, Multimodal contrast agent, Amyloid-β targeting, *In vivo* MR imaging.

ABSTRACT. Despite the wide use of magnetic resonance imaging (MRI) as a clinical diagnostic tool, there are still no clinically approved MRI contrast agents that can be applied for cerebral Alzheimer's disease (AD) biomarker imaging. We report here the design and development of the first amyloid-β (Aβ)-targeted, blood brain barrier (BBB) penetrable theranostic Gd(DOTA)-cyanine dyad, which was synthesized by the conjugation of Gd(DOTA) complex and carbazole-based cyanine dye by the copper(I)-catalyzed azide-alkyne cycloaddition click reaction, for imaging of Aβ *in vivo* and *ex vivo* in AD mouse models. This dyad, as a multimodal probe, possesses desirable multifunctional properties, including good biocompatibility, low cytotoxicity, high *Aβ* selectivity, strong fluorescence enhancement upon binding with Aβ species, good paramagnetic property, high stability, good BBB penetrability, and fast elimination from the mouse. The longitudinal relaxivity (r_1) of the dyad was found to be 4.42 mM^{-1} s^{-1} at 3 T suggesting its promise as a T_1-weighted MRI contrast agent. The probe has been successfully demonstrated to be able to apply for one- and two-photon excited fluorescence and MR imaging of Aβ in transgenic mouse models of AD. In addition, it can inhibit Aβ aggregation, protect against toxicity induced by Aβ and suppress Aβ-induced reactive oxygen species (ROS) production. Our results demonstrate its highly promising theranostic capability for diagnosis and therapy of AD and extraordinary potential for MRI of Aβ in humans.

1. INTRODUCTION

Alzheimer's disease (AD) is a progressive irreversible neurodegenerative disorder that causes problems with cognitive functions, memory, and behavior. Approximately 35 million people presently suffer from AD worldwide.[1] Even though drugs are currently available to offer symptomatic relief, disease-modifying therapy that can stop and reverse the disease is still lacking. Therefore, early detection, diagnosis and treatment could provide the best chance to deter and delay disease progression and deleterious damage. Currently, no single diagnostic test can be clinically used to confirm the onset of the disease.[2] AD is pathologically characterized by the accumulation of extracellular senile plaques that predominantly comprise insoluble amyloid-β (Aβ) deposits and intracellular neurofibrillary tangles that consist mainly of hyperphosphorylated microtubule-associated tau proteins. The deposition of cerebral amyloid plaques appears much earlier than any clinical symptoms, and it is widely believed that the process of Aβ aggregation is a causative event for the pathogenesis of AD and that Aβ is considered to be an important biomarker for disease screening and treatment monitoring.[3]

Among various detection approaches, advanced neuroimaging is an indispensable and powerful technique for the monitoring and diagnosis of disease progression, real-time visualization of brain-specific region changes, and evaluation of the treatment response of potential drugs.[4] In AD patients, cerebral Aβ plaques can be visualized by positron emission tomography (PET);[5] however, this method requires an invasive radiotracer, which results in limited spatial resolution and a high cost.[6-7] Therefore, it would not be suitable for routine and population-wide disease screening particularly in the pre-symptomatic stage.

Magnetic resonance imaging (MRI) is the most universally used clinical technique/tool for disease diagnostics due to its noninvasiveness, high temporal and spatial resolution, and deep tissue penetration.[8-10] Thus, it is the ideal imaging modality for the brain and nervous system. To overcome the intrinsic low sensitivity of MRI to Aβ plaques, a contrast agent is often employed to enhance the image contrast. Currently, there are no clinically approved MRI contrast agents that can be used for cerebral AD biomarker imaging in humans.[11] In addition, contrast agents that can be applied for real-time imaging Aβ plaques/species in animal models are still rather limited.[12-15]

Despite the occasional association with nephrogenic system fibrosis, most extensively clinically used MRI contrast agents are based on gadolinium(III) complexes such as Gd(DOTA) (DOTA = 1,4,7,10-tetraazacyclododecane-1,4,7,10-tetraacetic acid) and Gd(DTPA) (DTPA = diethylenetriaminepentaacetic acid), which advantageously offer positive (bright) image signals because of the high longitudinal relaxivity (r_1) values.[16] These complexes also exhibit good biostability and high inertness since free Gd(III) ions are toxic.[17] However, Gd(III) complexes have rarely been applied for MRI of Aβ species *in vivo* due to the poor blood brain barrier (BBB) penetrability and lack of Aβ specificity and targetability of the existing contrast agents.[18-20] The targeting ability of a contrast agent would substantially improve magnetic resonance (MR) image contrast in the region of interest and thus enhance the sensitivity and accuracy of detection of an agent.

Multimodal imaging probes are emerging due to their versatility, offering multiple imaging capabilities from a single administration in which various imaging techniques can provide enriched and complementary information about the imaging region of interest.[21-23] For AD, an optical/MR multi-modal imaging probe with sensitivity at the molecular level could enable imaging of Aβ species/plaques at various levels of organization e.g. from nanostructures to the entire plaques,

providing microscopic and macroscopic information to facilitate an investigation of the evolution of the disease and to evaluate the efficiency and mode of action of new therapeutic agents in animal models. To develop smart multimodal contrast agents with various imaging capabilities from MR and fluorescence (in the visible or near infrared (NIR) region) to two-photon excited fluorescence (TPEF) imaging of Aβ species *in vivo*, the use of Gd(III) complex-based molecules is of great practical advantages over the use of Gd-based nanoparticles, which often accumulate in the main organs of the reticuloendothelial system after administration, thus lessening the bioavailability in the brain and require longer renal elimination leading to the potential prolonged toxicity.[24] To convert a clinically used MRI-active Gd(III) complex into a desirable and practically useful Aβ multimodal imaging probe, a multifunctional vehicle molecule that is biocompatible, NIR emissive, two-photon absorption (TPA) active, BBB permeable and Aβ targetable could be integrated with it. In this work, we report the first BBB-permeable and Aβ-targeted Gd(III) complex-derived dyads synthesized by conjugation of Gd(DOTA) and carbazole-based cyanine[25] with different linkers, namely, Dyad-*n*, where n = 1-3 (Figure 1A), as multimodal contrast agents for imaging of Aβ species *in vivo* and *ex vivo* in the brains of mice in AD mouse models. Among the series, the facilely synthesized Dyad-3 was found to exhibit the most favorable functional properties, including good biocompatibility, low cytotoxicity, high Aβ selectivity, strong turn-on fluorescence upon interacting with Aβ species, large longitudinal relaxivity (r_1), high stability, good BBB penetrability, and fast elimination from the mouse, and was successfully applied for real-time multimodal imaging of Aβ species in a transgenic mouse model of AD. Furthermore, with the incorporation of carbazole-based cyanine, Dyad-3 exhibits effective inhibitory effect against Aβ aggregation, excellent protection against toxicity induced by Aβ, and good suppression of Aβ-induced reactive oxygen species (ROS) production, highlighting its remarkable promise as

a practical Aβ-targeted theranostic multimodal contrast agent for the diagnosis and treatment of AD.

2. EXPERIMENTAL SECTION

2.1 General procedures. All reagents and chemicals for the synthesis of dyad were commercially purchased and used without further purification unless otherwise stated. All the solvents purchased were dried by standard methods if necessary. Proton NMR spectra were recorded at 25 °C using a Bruker Avance-III - 400 and 500 NMR spectrometers and referenced to the residual $CHCl_3$ at 7.26 ppm, CD_3OD at 3.31 ppm or DMSO-d_6 at 2.5 ppm. Carbon NMR spectra were recorded using a Bruker-400 NMR spectrometer and referenced to the $CDCl_3$ at 77 ppm or DMSO-d_6 at 39.5 ppm. Mass Spectrometry (MS) measurements were performed using either fast atom bombardment (FAB) on an API ASTER Pulser I Hybrid Mass Spectrometer or matrix-assisted laser desorption ionization-time-of-flight (MALDI-TOF) technique on a Bruker Autoflex MALDI-TOF MS or electrospray ionization (ESI) technique on a Bruker Amazon SL instrument or on a Thermo Scientific MSQ Plus single quadrupole (parameter conditions for ESI-MS analysis: probe temperature: 350 °C, needle: 3.0 kV, detector: 1153 V and cone voltage: 200 V). UV-visible spectra were obtained either on a Varian Cary 50 scan using a rectangular quartz cell (Hellma, 100-QS with the cell dimension of 45 × 12.5 × 12.5 mm, path length of 10 mm and chamber volume of 3.5 mL) at 25 °C. Size-exclusion chromatography was carried out using a Bio-Beads® S-X3 support from Bio-Rad (#152-2750). HPLC measurements were conducted on a Dionex Ultimate 3000 system (Thermo Scientific) using C18 Chromolith® SpeedROD column (Merck, 2 μm, 50-4.6 mm) with a flow rate of 1.5 mL/min, injected volume of 30 μL and wavelength detection at 415 and 465 nm. Solvent A was 0.1% TFA in H_2O and solvent B was acetonitrile. Ion

chromatography analyses for TFA quantification were carried out on a Thermo Scientific Dionex ICS 5000 ion chromatograph equipped with a conductivity detector CD (Thermo Scientific Dionex) and a conductivity suppressor ASRS-ultra II 4 mm (Thermo Scientific Dionex).

2.2. Preparation of Aβ monomer, oligomer and fibril. Both A$\beta_{1\text{-}40}$ and A$\beta_{1\text{-}42}$ monomers were purchased from r-Peptide (USA) and used directly to prepare stock solutions without further purification. Literature procedures for the preparation of A$\beta_{1\text{-}40}$ and A$\beta_{1\text{-}42}$ oligomers and fibrils were followed, respectively.[26]

2.3. In-Vitro Binding Assays. Literature procedures for the determination of the dissociation constants of SL-N_3 and Dyad-3 with various Aβ samples (monomer, pre-formed oligomer and fibril) were followed.[26] Emission spectra of the mixture at different concentrations were measured by a HORIBA FluoroMax-4 Spectro Fluorometer using excitation wavelength of 497, 524 and 548 nm with emission ranges of 517-800, 544-800 and 568-800 nm for monomer, pre-formed oligomer and fibril, respectively.

2.4. Inhibition effect of SLN_3 and Dyad-3 on A$\beta_{1\text{-}40}$ and A$\beta_{1\text{-}42}$ fibrillation. The thioflavin T (ThT) fluorescence assay was adopted to evaluate the inhibitory effect of SLN_3 and Dyad-3 on A$\beta_{1\text{-}40}$ and A$\beta_{1\text{-}42}$ fibrillation. The time points selected were 0, 2, 6, 9, 15, 18, 21, 24, 27, and 30 h, respectively. Three independent experiments were performed. Data are expressed as the mean ± SD in the plot (n =3).[26]

2.5. Cell viability assays and neuroprotection study. The 3-(4,5-dimethyl-2-thiazolyl)-2,5-diphenyl-2H-tetrazolium bromide (MTT) assay was employed to study the cytotoxicity of SLN_3 and Dyad-3 on SH-SY5Y cells and literature protocols[27] were followed using 96-well plates at a density of 3×10^4 cells / well. In a neuroprotection study, SH-SY5Ycells were incubated with 10

μM of different neurotoxic compounds (including A$\beta_{1\text{-}42}$ monomers as controls) for 24 h. The SL-N_3 and Dyad-3 together with A$\beta_{1\text{-}42}$ monomer were seeded into the wells at 1 : 1 molar ratio. After seeding, the previously adopted MTT assay protocols were followed. The cytotoxicity results were calculated by the equation of ((MTT control – MTT bg) – (MTT inhibitor – MTT bg)) / (MTT control – MTT bg) × 100%. The relative cytotoxicity was calculated by the equation of (cytotoxicity in the presence of Dyad-3 and A$\beta_{1\text{-}42}$) / (cytotoxicity in the presence of A$\beta_{1\text{-}42}$ alone). Three independent experiments were conducted. Data are expressed as the mean ± SD of three independent experiments.

2.6. Reactive oxygen species (ROS) measurements. 2',7'-Dichlorodihydrofluorescein diacetate (DCFH-DA) assay was used to measure the ROS content in the treated cells. The previously adopted procedures[27] were followed using SH-SY5Y cells, DCFH-DA (Molecular Probes, life technologies, USA) and 96-well black culture plates (PerkinElmer). After being incubated with DCFH-DA, the treated cells were mixed with A$\beta_{1\text{-}42}$ monomer as a control. Meanwhile, SL-N_3 and Dyad-3 were mixed with A$\beta_{1\text{-}42}$ monomer in a 1:1 molar ratio, respectively. The relative ROS level was calculated by the equation of (ROS level in the presence of Dyad-3 and A$\beta_{1\text{-}42}$) / (ROS level in the presence of A$\beta_{1\text{-}42}$ alone). Data points are expressed as the mean value ± standard deviation of three independent experiments.

2.7. Animal experiments. Prior approval were obtained for all animal experiments from the Committee on the Use of Human and Animal Subjects in Teaching and Research (HASC) of Hong Kong Baptist University. Animal license to conduct the experiments were also obtained from the Department of Health, Hong Kong under the animal license no. (17-77) in DH/SHS/8/2/6 Pt.1. All methods and experiments were conducted in accordance with the approved guidelines and regulations. The 5XFAD transgenic mice purchased from the Jackson Laboratory (Bar Harbor,

ME, USA) were used in the imaging experiment.

In the MRI study, the double transgenic (APP/PS1) model mice were purchased from Beijing Hufukang Bioscience CO. INC. These experiments were carried out in accordance with institutional animal use and care regulations, according to protocol No. SYXK (Xiang) 2008−0001, approved by the Laboratory Animal Center of Hunan. Great effort has been taken to reduce the number of animals used and to minimize animal suffering.

2.8. *In vivo* NIRF imaging of Dyad. Before background imaging, 5XFAD transgenic mice (12 months old) and age-matched wild-type mice were shaved as the controls. Before imaging, oxygen (1.0 mL) was supplemented with isoflurane gas (2.0 mL min^{-1}). The mice were anesthetized under theses condition, kept still, and then injected with 100 μL of Dyad-3 (10 mg/kg) through the tail vein. The IVIS imaging system was used to collect fluorescence images from the brain at different time points. A filter set (excitation at 496 nm and emission at 690-700 nm) was used to obtain a fluorescent image with an exposure time of 1 s. Living Image software was used to analyze the image and select the ROI in the brain area. The brain fluorescence intensity obtained at each time point was normalized to the background fluorescence intensity of each mouse (i.e. F(t)/F(pre)), where F(t) is the fluorescence signal at the specific time point and F(pre) is the background fluorescence intensity. Data points are expressed as the mean value ± standard deviation of three independent mice.

2.9. Co-staining brain tissues of 5XFAD-Tg mice *ex vivo*. 5XFAD transgenic mice were tail-vein injected with Dyad-3. After 30 minutes, it was deeply anesthetized and perfused intracranially with PBS, and then perfused with 8% formaldehyde in PBS (pH 7.4). After excision, the brain was buried in the optimal cutting temperature (OCT) compound, and then the slice was frozen with a

cryostat (thickness 10 μm). Then, 0.4% Triton X-100 was used to infiltrate the free-floating portion and block in a blocking solution containing 2% BSA. For staining with Thio-S dye, the sections were incubated with 1.0 μM Thio-S solution for 5-8 minutes, then washed with 25% ethanol for 4 minutes, then washed with PBS for 5 minutes, and then washed in water for 5 minutes. For co-staining studies, free-floating sections were further incubated with primary antibodies, 4G8, and 6E10 (1:200) at 4°C overnight. The sections were washed in PBS and incubated in a 2% BSA solution containing goat anti-mouse or goat anti-rabbit secondary antibodies conjugated with Alexa Fluor 488 (1:500) at room temperature for 2 h. A confocal laser scanning microscope (Leica TCS SP8) was used to sequentially capture images of Aβ immunofluorescence reactivity, followed by images of Dyad-3 on Aβ species.

2.10. Measurement of relaxation rates of Dyad-3. Various Dyad-3 concentrations (0.0196, 0.0391, 0.0782, 0.1563, 0.3125, 0.6250, 1.25, and 2.5 mM) in aqueous solution were prepared firstly, and then T_1 and T_2 relaxation rates (R_1 and R_2) were measured on the same Siemens Prisma 3.0 T MR Scanner. T_1 values was obtained using Inversion Recovery (IR) pulse sequence with inversion time point at 25, 50, 100, 200, 400, 800, 1600 and 3200 ms. T_2 values were obtained using Carr-Purcell-Meiboom-Gill sequence (CPMG) pulse sequence with different echo times.

2.11. Two-photon absorption measurements. The two photon excitation spectra were measured according to the previously published protocols[28] using rhodamine B in MeOH in the range of 750-880 and 930-1000 nm and fluorescein in 0.1 N NaOH solution in the range 880-930 nm as a calibration reference.

2.12. Magnetic resonance imaging of Dyad-3 *in vivo*. *In-vivo* T_1-weighted images of 6-month-old 2xTg-AD and age-matched WT mice before and after 90 min post-injection of Dyad-3 *via* tail

vein at different depths (every 10 μm apart). The MRI was performed on a Siemens Prisma 3.0 T MR scanner (Erlangen, Germany) with gradient strength up to 80 mT/m and 7.0 T MR Scanner, and a small animal surface coil. The MRI scan parameters were: TR = 1000 ms TE = 11 ms, NEX = 8, FOV = 20*20 mm, Matrix = 256*256.

3. RESULTS AND DISCUSSION

To synthesize biocompatible and tractable Gd(DOTA)-based dyads for neuroimaging applications, the copper(I)-catalyzed azide-alkyne cycloaddition click reaction was adopted as a key step to conjugate Gd(DOTA) with carbazole-based cyanine using two different linking approaches (Figure 1B). Scheme S1 outlines the overall synthetic route for the preparation of Gd(DOTA)-based dyads, namely, Dyad-*n*, where n = 1-3. Because of the facile synthesis and ease of purification of the resulting Gd (III) complex-based dyad, the click chemistry linking DOTA-Gd-alkyne and SL-N_3 is a more viable and reproducible method for large-scale synthesis. These dyads were fully characterized by various spectroscopic techniques including ^{1}H NMR, ^{13}C NMR, and HRMS. Based on the spectroscopic data, the corresponding structures were in good agreement with them. (see Supporting Information for details) It is worth mentioning that the counteranion provides a useful tool to enhance the solubility of the dyad in aqueous medium. Upon exchanging the halide counteranion with trifluoroacetate, Dyad-3 exhibits superior solubility in PB buffer, greatly facilitating its bioapplications.

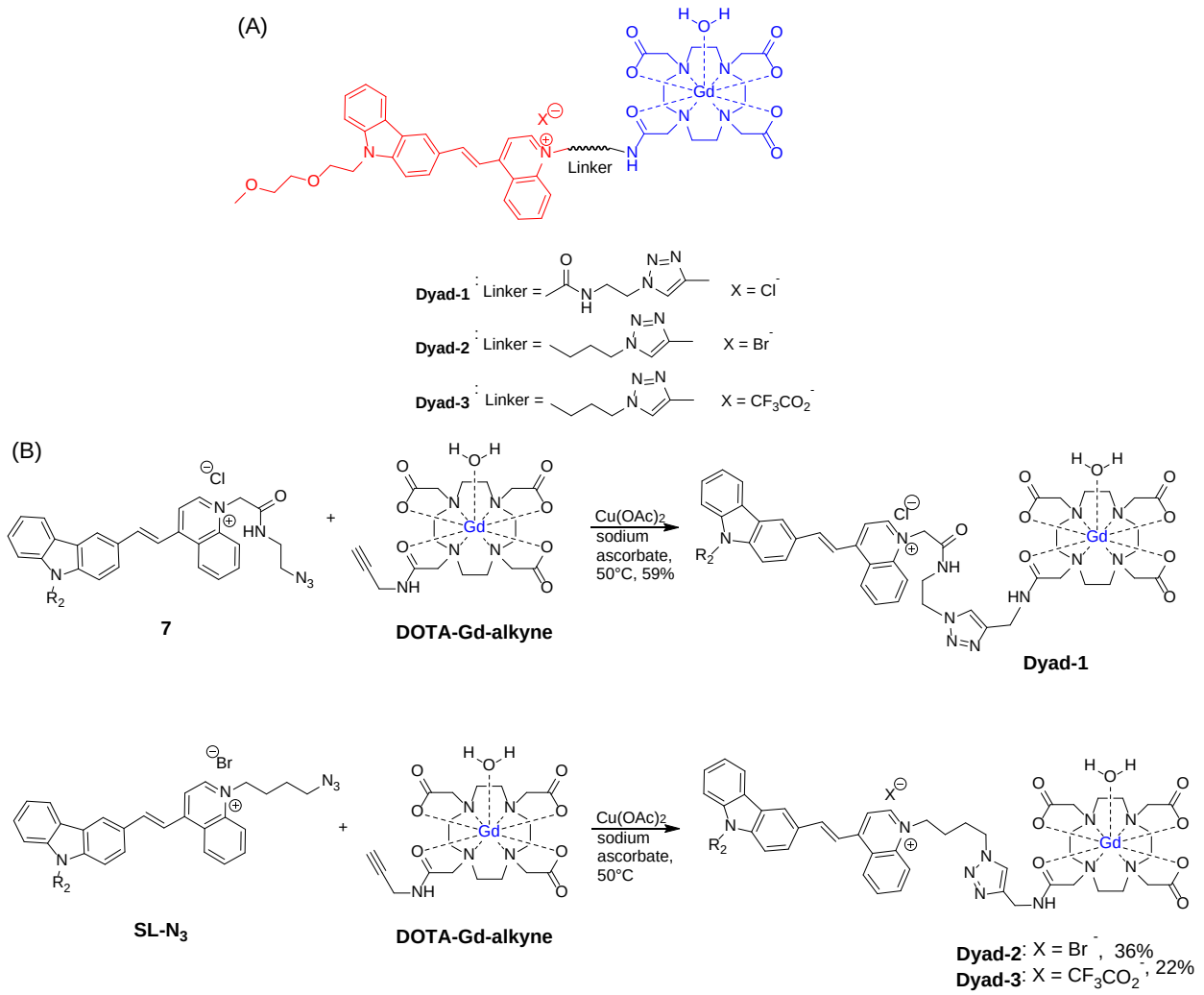

Figure 1. (A) Molecular structures of Gd(DOTA)-based dyads, Dyad-*n* (*n* = 1-3) where fluorescent carbazole-based cyanine and magnetically active Gd(DOTA) are highlighted in red and blue, respectively. (B) Copper(I)-catalyzed azide-alkyne cycloaddition click reaction for the synthesis of Gd(DOTA)-cyanine dyads.

These Gd(DOTA)-conjugated cyanine dyads showed a strong absorption band at ~463-490 nm and a weak emission spanning the range of 634-650 nm with low fluorescence quantum yields in different solvents (e.g., Φ_{PL} = 0.0057 in PB buffer) (Figure S1 and Table S1), and these bands

were mainly attributed to the donor-acceptor intramolecular charge transfer of the carbazole-based cyanine moiety. In addition, Dyad-3 exhibited strong TPEF when excited at above 800 nm with a maximum two-photon brightness ($\delta_2\Phi$) of ~210 GM at 950 nm (Figure S2), which was highly desirable for achieving good contrast and high brightness in TPEF bioimaging. Upon addition to Aβ species, Dyad-3 exhibited strong turn-on fluorescence concomitant with a blue-shift in the emission spectrum (Figure S3), indicating binding between the cyanine moiety of the dyad and Aβ. Such binding interactions were highly selective towards Aβ over various biorelated metal ions and bioactive molecules (Figure S4). The binding affinity of Dyad-3 towards various Aβ species was evaluated by fluorescence titration, and the results indicated reasonably strong binding interactions, with a dissociation constant, K_d, in the range of 90-300 μM in 10% DMSO buffer solution (Table S2). It is worth noting that the K_d value depends on the solvent and evaluation method. Dyad-3 also shows excellent pH stability, with no significant alteration of the fluorescence response over a wide range of pH values in the presence and absence of Aβ (Figure S5), which is a prerequisite for imaging Aβ *in vivo*.

Because biocompatibility is essential to bioapplications, the cytotoxicity of the Gd(DOTA)-based dyad was first evaluated by MTT assay, which indicated a very low toxicity towards SH-SY5Y cells, with lethal concentration 50% (LC_{50}) = ~ 238 μM (Figure S6). The biodistribution of Dyad-3 in different organs in mice over time was also evaluated by measuring and monitoring the fluorescence emission of the dyad after being tail-vein injected with the dyad for 2, 12, 24, and 48 h. As clearly shown in the fluorescence images (Figure S7), the dyad was mainly distributed in the liver, kidney, lung, and brain 2 h after injection, suggesting that the dyad was BBB penetrable and likely eliminated through the hepatic and renal metabolism. The fluorescence intensity diminished substantially 12 h after injection. Then, 24 h postinjection, the fluorescence signal almost

completely disappeared in all the organs (Figure S8), indicating a fast washout from the mouse body, which is essential and beneficial to minimize the potential risk of prolonged biotoxicity of the dyad.

To further confirm the BBB penetrability and investigate the real-time imaging capability of Dyad-3, the fluorescence signals of dyads in the brains of 12-month-old 5XFAD transgenic (Tg) mice that overexpressed Aβ species and age-matched wild-type (WT) mice were monitored *in vivo* and compared after they were injected with Dyad-3 via the tail vein. As clearly seen in Figure 2A and S9A, the fluorescence reached a maximum after 90 min of injection and were much intense in the brain of the Tg mouse as compared to that in the WT one at all the time points. The strongly increased fluorescence in the Tg mouse was due to the strong Aβ binding-induced fluorescence enhancement of Dyad-3 in the Tg mouse. Furthermore, such a strong interaction of the dyad with cerebral Aβ plaques resulted in a longer retention and washout time for the Tg mouse. As evidenced by the HPLC-ESI-MS analysis of the brain extract of the dyad-treated mice 2 and 12 h after injection, the intact dyad molecule was detected. All these results consistently demonstrated the BBB permeability, Aβ targetability and *in vivo* biostability in the brain of the mice of Dyad-3. To further prove the targeting capability of Gd(DOTA)-based dyads toward cerebral Aβ, co-staining studies on dyad-treated 5XFAD Tg mouse brain slices with Aβ-specific 6E10 and 4G8 antibodies as well as the Aβ plaque-specific thioflavin-S (Thio-S) dye were conducted. As seen in *ex vivo* images of brain slices of Tg mice upon one-photon and two-photon excitations, the blue or red fluorescence clusters of the dyad colocalize well with the green fluorescence of Thio-S (Figure 2B), 4G8, and 6E10 (Figure S9B), unanimously confirming the Aβ-targeting capability of this dyad in the brains of the Tg mice. In brief, Dyad-3 was shown to be an effective Aβ-targeted

fluorescence probe for imaging of Aβ species *ex vivo* and *in vivo* in the brain of an AD mouse model under one-photon and two-photon excitation.

(A)

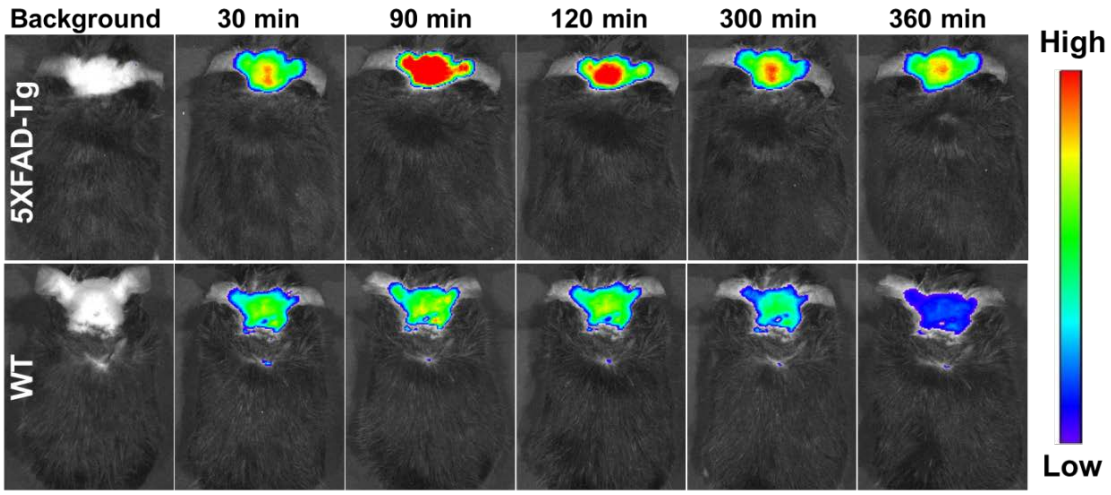

(B)

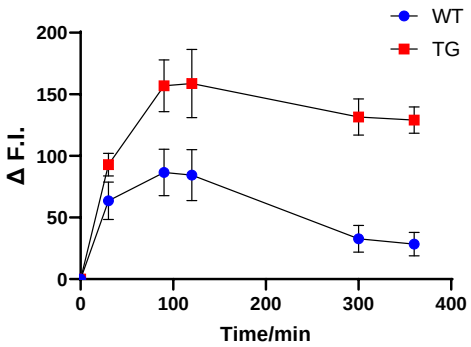

(C)

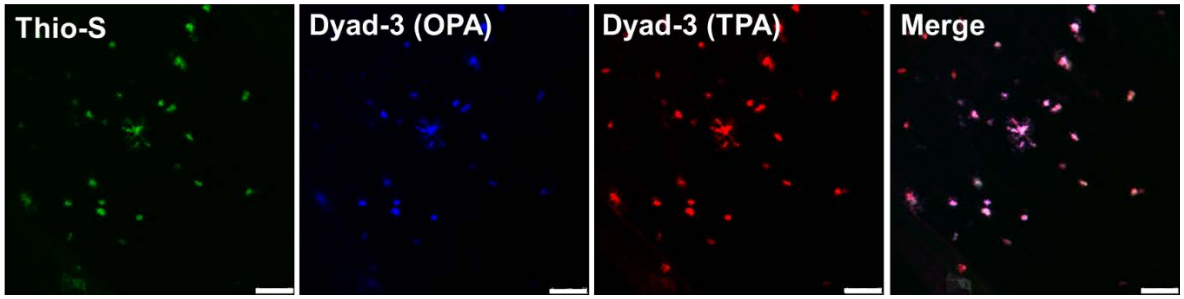

Figure 2. (A) *In vivo* fluorescence images of 12-month old 5XFAD Tg and age-matched WT mice before and after administered with Dyad-3 (100 μL, 20 mg kg^{-1}) in 10% DMSO PB (0.5 M, pH = 7.4) via tail vein at different time points and λ_{ex} = 465 nm, λ_{em} = 600−760 nm. (B) The plot of the relative fluorescence signals [F(t)/F(pre)] monitored in real-time of 12-month old 5XFAD Tg and age-matched WT mice before and after administered with Dyad-3 at different time points. Data are expressed as the mean ± SD of three independent mice (n = 3). (C) *Ex vivo* images of the brain slices of 5XFAD Tg-mouse excited by one-photon (OPA) and two-photon (TPA) excitation (λ_{ex} = 950 nm) co-stained with Thio-S. Scale bar: 50 μm.

To evaluate the magnetic resonance properties of Dyad-3, the longitudinal (r_1) and transverse (r_2) relaxivities, determined by plotting the proton spin-lattice ($1/T_1$) and spin-spin ($1/T_2$) relaxation rates as a function of the dyad concentration measured on a 3.0 T magnetic resonance scanner, were found to be 4.42 and 0.61 mM^{-1} s^{-1}, respectively (Figure 3A and S10). This result demonstrated the promise of this dyad for T_1-weighted MRI applications.

The use of this dyad as a T_1-weighted MRI contrast agent for Aβ imaging *in vivo* was first carried out on a 10-month-old double Tg, APP/PS1 mouse after tail-vein injection of Dyad-3. The MR images recorded on a 3.0 T MR scanner at different time intervals are shown in Figure S11A. As clearly seen, the *in vivo* T_1-weighted MR pseudo-color mapped brain images of the Tg mouse became brighter and brighter over a period of 90-min as compared to those of the pre-injected ones indicating the BBB permeability of the dyad and consistent to the results of the fluorescence imaging. The *in vivo* MR images at different depths after 90-min post-injection of Dyad-3 were also recorded. There are brighter areas or spots that are found in different depths of the Tg brain as shown in Figure S11B, indicating the regions where the dyad and Aβ reside. Furthermore, Figure 3 and S12 show *in vivo* T_1-weighted MR images of 6-month-old double Tg, APP/PS1 and

WT mice before injection and 30 min post-injection of dyad at different depths via the tail vein measured by 7.0 T MR scanner. These results unambiguously confirm that the postinjected images are brighter at different depths of the brain than the preinjected images, in sharp contrast to those from the WT mice, demonstrating the capability of this dyad to serve as an effective and sensitive T_1-weighted MRI contrast agent for cerebral Aβ imaging *in vivo*.

(A)

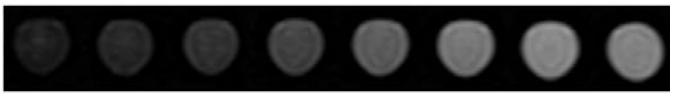

(B)

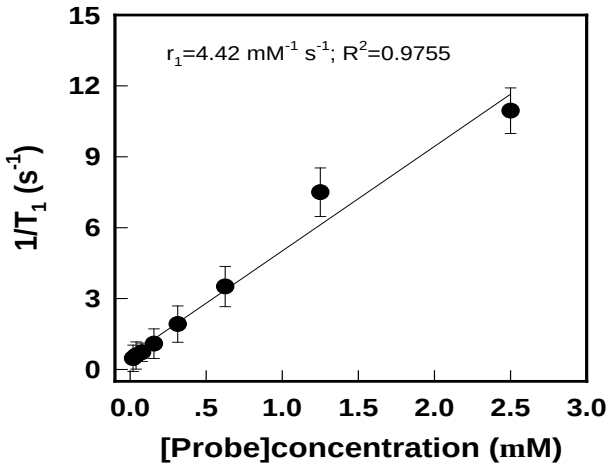

(C)

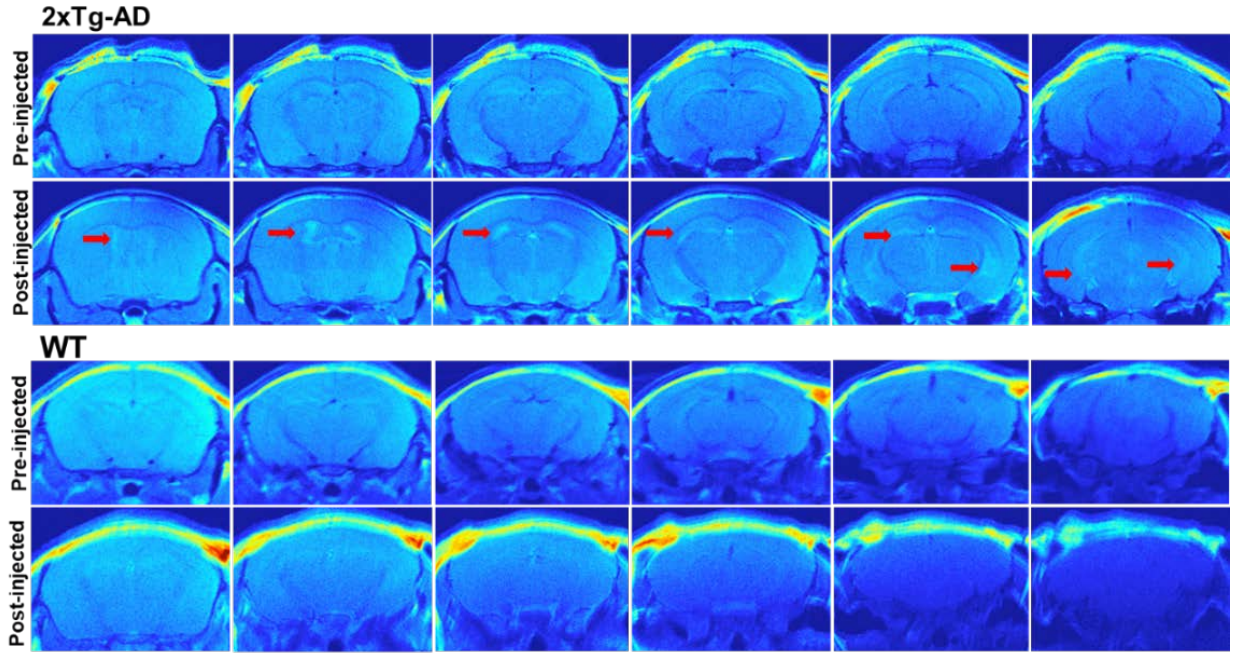

Figure 3. (A) The T_1-weighted MR images of Dyad-3 in aqueous solution at various concentrations (0.0196, 0.0391, 0.0782, 0.1563, 0.3125, 0.6250, 1.25, and 2.5 mM, respectively). (B) Plot of $1/T_1$ as a function of different probe concentrations measured on a 3T magnetic resonance scanner. Data are expressed as the mean ± SD of six replicates (n = 6). (C) *In vivo* T_1-weighted MR pseudo-color mapped images of 6-month-old double Tg-AD and age-matched WT mice before and after injection of Dyad-3 via tail vein at different depths in which the images were taken every 10 μm apart after 90 min post-injection of probe on a Siemens Prisma 7.0 T MR scanner.

Soluble Aβ aggregates have been shown to be neurotoxic and one of the important causative factors in AD pathogenesis; therefore, molecule/material capable of inhibiting Aβ aggregation would offer therapeutic potential to treat AD. Remarkably, Dyad-3 could also effectively inhibit self-aggregation of Aβ, as evidenced by the thioflavin T (ThT) fluorescence assay (Figure 4A) with inhibition concentration 50% (IC_{50}) value of 2.83 μM, suggesting that this dyad holds great

potential for AD intervention. In addition to low cytotoxicity, the dyad was found to be able to protect against the toxicity induced by the Aβ species toward SH-SY5Y cells. There was a ~10-30% decrease in the cytotoxicity induced by various $A\beta_{42}$ species in the presence of Dyad-3. (Figure 4B) Studies showed that one of the causes of Aβ-induced neurotoxicity was the overproduction of ROS. As shown in Figure 4C, in the presence of Dyad-3, there was a substantial decrease of ~30-65% in ROS production induced by various $A\beta_{1\text{-}42}$ species. Such an effective inhibition of ROS generation further highlighted its potent neuroprotective effect and its tremendous promise as a therapeutic for AD. Thus, Dyad-3 is a highly versatile theranostic multimodal contrast agent for AD.[29]

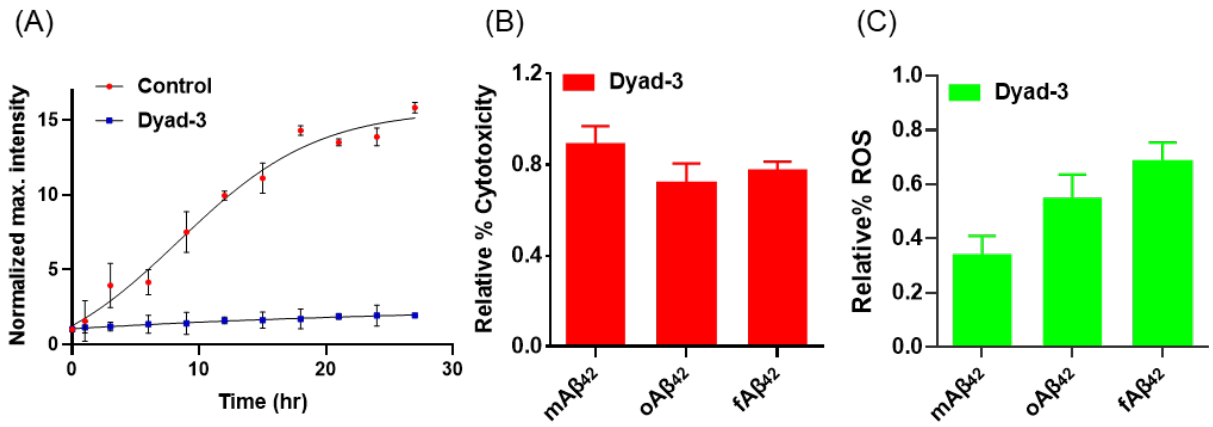

Figure 4. (A) Plot of the fluorescence intensity of ThT measured at 490 nm after incubation of $A\beta_{42}$ monomer at different time points in the absence and the presence of Dyad-3. Data points are expressed as the mean value ± standard deviation of three independent experiments. (B) Plot of relative cytotoxicity of SH-SY5Y cells in the presence of Dyad-3 against $A\beta_{42}$ monomers, oligomers and fibrils, respectively. The relative cytotoxicity was calculated by the equation: (cytotoxicity in the presence of Dyad-3 and $A\beta_{1\text{-}42}$)/ (cytotoxicity in the presence of $A\beta_{42}$ alone). Data are expressed as the mean ± SD of three independent experiments. (C) Plot of the relative

ROS levels for SH-SY5Y cells in the presence of Dyad-3 and $A\beta_{1-42}$ monomers, oligomers and fibrils, respectively. The relative ROS level was calculated by the equation: (ROS level in the presence of Dyad-3 and $A\beta_{1-42}$)/ (ROS level in the presence of $A\beta_{42}$ alone). Data points are expressed as the mean ± standard derivation of three independent experiments.

4. CONCLUSIONS

In summary, an Aβ-targeted theranostic Gd(DOTA)-cyanine dyad has been successfully designed, developed and demonstrated for the first time as a multimodal contrast agent for imaging of cerebral Aβ *in vivo* and *ex vivo* in AD mouse models. Upon conjugation of the carbazole-based cyanine with Gd(DOTA), the novel dyad is Aβ specific and targetable, NIR emissive, two-photon absorption (TPA) active, and BBB permeable. This dyad has been demonstrated not only to be useful and sensitive for fluorescence (NIR), TPEF and MR imaging of Aβ species in AD mouse models but also to be able to effectively inhibit self-aggregation of Aβ, protect against Aβ-induced toxicity and suppress ROS production, signifying its outstanding promise as a practical Aβ-targeted theranostic multimodal contrast agent for the diagnosis and treatment of AD. This work has demonstrated an alternative and practical approach to develop multimodal probes for imaging the hallmarks of AD. The success of this development has also highlighted the extraordinary potential of this effective and sensitive contrast agent for MRI of Aβ in humans.

ASSOCIATED CONTENT

Supporting Information. The following files are available free of charge.

The Supporting Information is available free of charge, including detailed synthetic procedures, optical spectra, two-photon excited spectrum, fluorescence titration plots, results of interference and photostability studies, MTT assays results, biodistribution results, *in vivo* and *ex vivo*

images, *in vivo* MR images, inhibition assay results, and spectra for compounds characterization. Scheme S1. Figures S1 to S22. Tables S1 to S2 (PDF)

AUTHOR INFORMATION

Corresponding Author

Man Shing Wong − Department of Chemistry, Hong Kong Baptist University, Kowloon Tong, Hong Kong, SAR China. E-mail: mswong@hkbu.edu.hk

ORCID: 0000-0001-8141-9791

Claude P. Gros − ICMUB (UMR CNRS 6302), Université Bourgogne Franche-Comté, 21000 Dijon, France. E-mail: Claude.Gros@u-bourgogne.fr

ORCID: 0000-0002-6966-947X

Frédéric Bolze − Conception et Applications des Molécules Bioactives (UMR CNRS-Unistra 7199), Faculté de Pharmacie, Université de Strasbourg, 74 route du Rhin, 67401 Illkrich, France. E-mail: frederic.bolze@unistra.fr

ORCID: 0000-0002-7955-4668

Yinhui Li − Key Laboratory for Green Organic Synthesis and Application of Hunan Province, Key Laboratory of Environmentally Friendly Chemistry Application of Ministry of Education, College of Chemistry, Xiangtan University, Xiangtan 411105, China. Email: yinhuili16@163.com

Hung Wing Li − Department of Chemistry, The Chinese University of Hong Kong, Shatin, Hong Kong, SAR China. E-mail: hungwingli@cuhk.edu.hk

ORCID: 0000-0003-4840-1965

Funding Sources

The authors acknowledge the financial support through General Research Fund (HKBU12302620) of Research Grants Council of Hong Kong, the National Natural Science Foundation of China (21675135 and 21974119), Interdisciplinary Research Clusters Matching Scheme (IRCMS-19-20-H02A), Research Committee of Hong Kong Baptist University, and Hunan Provincial Natural Science Foundation of China (2019JJ30020). This work is part of the MULTIMOD project, supported by the Conseil Régional de Bourgogne Franche Comté and the European Union through the PO FEDER-FSE Bourgogne 2014/2020 programs.

Notes

The authors declare no competing financial interest.

ACKNOWLEDGMENT

We are really thankful to Mrs Sandrine Pacquelet for technical assistance. The authors also thank the Plateforme d'Analyse Chimique et de Synthèse Moléculaire de l'Université de Bourgogne (PACSMUB, http://www.wpcm.fr) for access to analytical instrumentation. We are thankful to Dr Quentin Bonnin and Mrs Marie-José Penouilh for HR-MS measurements and Dr. Myriam Laly for the determination of TFA content in the samples purified by semi-preparative RP-HPLC and to Dr Frédéric Boschetti and CheMatech Company (Dijon, France) for his advice and precious expertise concerning the propargyl-DOTA-tris(*t*-Bu) ester precursor. We are also grateful to Prof. Min Li and Dr. Iyaswamy Ashok for an offer of the 5XFAD transgenic mice and assistance for the fluorescence imaging experiments at the School of Chinese Medicine, Hong Kong Baptist University. This work has constituted part of the Ph.D. dissertation of Xueli Wang at Hong Kong Baptist University.

REFERENCES

1. Laske, C., Phase 3 Trials of Solanezumab and Bapineuzumab for Alzheimer's Disease. *New England Journal of Medicine* **2014**, *370* (15), 1459-1460.

2. Yang, J.; Zhao, X.; Lu, X.; Lin, X.; Xu, G., A Data Preprocessing Strategy for Metabolomics to Reduce the Mask Effect in Data Analysis. *Front Mol Biosci* **2015**, *2*, 4.

3. Singh, S. K.; Srivastav, S.; Yadav, A. K.; Srikrishna, S.; Perry, G., Overview of Alzheimer's Disease and Some Therapeutic Approaches Targeting Abeta by Using Several Synthetic and Herbal Compounds. *Oxid Med Cell Longev* **2016**, *2016*, 7361613.

4. Limperopoulos, C., Advanced Neuroimaging Techniques: their Role in the Development of Future Fetal and Neonatal Neuroprotection. *Semin Perinatol* **2010**, *34* (1), 93-101.

5. Vlassenko, A. G.; Benzinger, T. L.; Morris, J. C., PET Amyloid-Beta Imaging in Preclinical Alzheimer's Disease. *Biochim Biophys Acta* **2012**, *1822* (3), 370-9.

6. Zhu, X.; Gao, H.; Zan, W.; Li, Y.; Zhang, J.; Liu, X.; Wei, X.; Qi, F.; Yao, X.; Zhang, H., A Rational Designed Thiols Fluorescence Probe: the Positional Isomer in PET. *Tetrahedron* **2016**, *72* (16), 2048-2056.

7. Vaquero, J. J.; Kinahan, P., Positron Emission Tomography: Current Challenges and Opportunities for Technological Advances in Clinical and Preclinical Imaging Systems. *Annu Rev Biomed Eng* **2015**, *17*, 385-414.

8. Na, H. B.; Song, I. C.; Hyeon, T., Inorganic Nanoparticles for MRI Contrast Agents. *Advanced Materials* **2009**, *21* (21), 2133-2148.

9. Zhang, Y.; Zhu, X.; Liu, L.; Hong, S.; Zuo, Z.; Wang, P.; Su, D., Synthesis and In Vitro Study of a Dual-Mode Probe Targeting Integrin $Alpha_v$ $Beta_3$. *Nanoscale Res Lett* **2018**, *13* (1), 281.

10. Zhu, D.; Liu, F.; Ma, L.; Liu, D.; Wang, Z., Nanoparticle-Based Systems for T(1)-Weighted Magnetic Resonance Imaging Contrast Agents. *Int J Mol Sci* **2013**, *14* (5), 10591-607.

11. Wahsner, J.; Gale, E. M.; Rodriguez-Rodriguez, A.; Caravan, P., Chemistry of MRI Contrast Agents: Current Challenges and New Frontiers. *Chem Rev* **2019**, *119* (2), 957-1057.

12. Zhou, J.; Fa, H.; Yin, W.; Zhang, J.; Hou, C.; Huo, D.; Zhang, D.; Zhang, H., Synthesis of Superparamagnetic Iron Oxide Nanoparticles Coated with a DDNP-Carboxyl Derivative for In Vitro Magnetic Resonance Imaging of Alzheimer's Disease. *Mater Sci Eng C Mater Biol Appl* **2014**, *37*, 348-55.

13. Zhang, D.; Fa, H. B.; Zhou, J. T.; Li, S.; Diao, X. W.; Yin, W., The Detection of Beta-Amyloid Plaques in an Alzheimer's Disease Rat Model with DDNP-SPIO. *Clin Radiol* **2015**, *70* (1), 74-80.

14. Li, Y.; Xu, D.; Chan, H. N.; Poon, C. Y.; Ho, S. L.; Li, H. W.; Wong, M. S., Dual-Modal NIR-Fluorophore Conjugated Magnetic Nanoparticle for Imaging Amyloid-Beta Species In Vivo. *Small* **2018**, *14* (28), e1800901.

15. Wang, C.; Wang, X.; Chan, H. N.; Liu, G.; Wang, Z.; Li, H. W.; Wong, M. S., Amyloid-β Oligomer-Targeted Gadolinium-Based NIR/MR Dual-Modal Theranostic Nanoprobe for Alzheimer's Disease. *Advanced Functional Materials* **2020**, *30* (16).

16. Ota, T.; Kimura, J.; Ishiguchi, T., Safety and Clinical Usefulness of Gadoteric Acid Including Post-Marketing Surveillance. *Imaging in Medicine* **2012**, *4* (4), 397-409.

17. Rogosnitzky, M.; Branch, S., Gadolinium-Based Contrast Agent Toxicity: a Review of Known and Proposed Mechanisms. *Biometals* **2016**, *29* (3), 365-76.

18. Martins, A. F.; Oliveira, A. C.; Morfin, J. F.; Laurents, D. V.; Toth, E.; Geraldes, C. F., Associating a Negatively Charged GdDOTA-Derivative to the Pittsburgh Compound B for

Targeting Abeta-Amyloid Aggregates. *J Biol Inorg Chem* **2016**, *21* (1), 83-99.

19. Vithanarachchi, S. M.; Allen, M. J., A Multimodal, Beta-Amyloid-Targeted Contrast Agent. *Chem Commun (Camb)* **2013**, *49* (39), 4148-50.

20. Montagne, A.; Toga, A. W.; Zlokovic, B. V., Blood-Brain Barrier Permeability and Gadolinium: Benefits and Potential Pitfalls in Research. *JAMA Neurol* **2016**, *73* (1), 13-4.

21. Jin, R.; Lin, B.; Li, D.; Ai, H., Superparamagnetic Iron Oxide Nanoparticles for MR Imaging and Therapy: Design Considerations and Clinical Applications. *Curr Opin Pharmacol* **2014**, *18*, 18-27.

22. Hou, Y.; Qiao, R.; Fang, F.; Wang, X.; Dong, C.; Liu, K.; Liu, C.; Liu, Z.; Lei, H.; Wang, F.; Gao, M., $NaGdF_4$ Nanoparticle-Based Molecular Probes for Magnetic Resonance Imaging of Intraperitoneal Tumor Xenografts In Vivo. *ACS Nano* **2013**, *7* (1), 330-8.

23. Fan, W.; Shen, B.; Bu, W.; Zheng, X.; He, Q.; Cui, Z.; Ni, D.; Zhao, K.; Zhang, S.; Shi, J., Intranuclear Biophotonics by Smart Design of Nuclear-Targeting Photo-/Radio-Sensitizers Co-loaded Upconversion Nanoparticles. *Biomaterials* **2015,** *69*, 89-98.

24. Choi, G.; Kim, H.-K.; Baek, A. R.; Kim, S.; Kim, M. J.; Kim, M.; Cho, A. E.; Lee, G.-H.; Jung, H.; Yang, J.-u.; Lee, T.; Chang, Y., Multifunctional Imaging of Amyloid-Beta Peptides with a New Gadolinium-Based Contrast Agent in Alzheimer's Disease. *Journal of Industrial and Engineering Chemistry* **2020,** *83*, 214-223.

25. Yang, W.; Wong, Y.; Ng, O. T. W.; Bai, L.-P.; Kwong, D. W. J.; Ke, Y.; Jiang, Z.-H.; Li, H.-W.; Yung, K. K. L.; Wong, M. S., Inhibition of Beta-Amyloid Peptide Aggregation by Multifunctional Carbazole-Based Fluorophores. *Angewandte Chemie* **2012,** *124* (8), 1840-1846.

26. Li, Y.; Xu, D.; Sun, A.; Ho, S.-L.; Poon, C.-Y.; Chan, H.-N.; Ng, O. T. W.; Yung, K. K. L.; Yan, H.; Li, H.-W.; Wong, M. S., Fluoro-Substituted Cyanine for Reliable in vivo Labelling

of Amyloid-β Oligomers and Neuroprotection against Amyloid-β Induced Toxicity *Chem. Sci.* **2017**, *8*, 8279–8284.

27. Wang, X.; Wang, C.; Chan, H.-N.; Ashok, I.; Krishnamoorthi, S. K.; Li, M.; Li, H.-W.; Wong, M. S. Amyloid-β Oligomer Targeted Theranostic Probes for In Vivo NIR Imaging and Inhibition of Self-Aggregation and Amyloid-β Induced ROS Generation *Talanta* **2021**, *224*, 121830.

28. Auvray, M; Bolze, F.; Clavier, G.; Mahuteau-Betzer, F., Silafluorene as a Promising Core for Cell-Permeant, Highly Bright and Two-Photon Excitable Fluorescent Probes for Live-Cell Imaging *Dyes and Pigments* **2021**, 109083.

29. Wang, X. Organic Molecules for Diagnosis and Therapy of Alzheimer's Disease, Ph.D. Dissertation, Hong Kong Baptist University, Hong Kong, 2020.

SYNOPSIS